Nonlinear Apodization for Sidelobe Control in SAR Imagery

H. C. STANKWITZ
R. J. DALLAIRE
J. R. FIENUP, Senior Member, IEEE
Environmental Research Institute of Michigan

Synthetic aperture radar (SAR) imagery often requires sidelobe control, or *apodization*, via weighting of the frequency domain aperture. This is of particular importance when imaging scenes containing objects such as ships or buildings having very large radar cross sections. Sidelobe improvement using spectral weighting is invariably at the expense of mainlobe resolution.

Presented here is a class of nonlinear operators which significantly reduce sidelobe levels without degrading mainlobe resolution. Implementation is via sequential nonlinear operations applied to complex-valued (undetected) SAR imagery.

SAR imaging is used to motivate the concepts developed in this work. However, these nonlinear apodization techniques have potentially broad and far-ranging applications in antenna design, sonar, digital filtering, etc., i.e., whenever data can be represented as the Fourier transform of a finite-aperture signal.

Manuscript received December 22, 1992; revised July 14, 1993.

IEEE Log No. T-AES/31/1/07998.

Authors' address: Environmental Research Institute of Michigan, P.O. Box 134001, Ann Arbor, MI 48113-4001.

I. INTRODUCTION

Synthetic aperture radar (SAR) image formation processing [1] is illustrated in Fig. 1. Typically, a series of coherent linear-FM pulses is transmitted and received. At the receiver, the pulses are deramped and digitized. A complex-valued image is produced from the received pulses by a digital processor. The overall process, starting with the generation of coherent pulses and ending with a displayed image, is referred to as the "image chain."

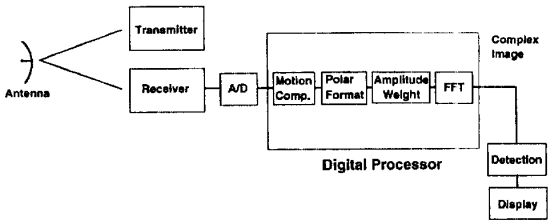

Fig. 1. SAR image chain.

The first step in digital processing is compensation of the received pulses for vehicle motion to maintain pulse-to-pulse coherence. In most fine-resolution SAR systems, this is followed by polar formatting [4] including polar-to-rectangular interpolation. At this point, the data and the complex image form a two-dimensional (2-D) Fourier transform pair. Sidelobe control is accomplished via amplitude weighting applied to the 2-D data "aperture" prior to the Fourier transform (FFT). The complex image is then detected and displayed in some manner (e.g., a CRT).

A bright point target in the scene will have a complex image representation given by the *impulse response* (IPR) of the system. For a uniform weighting function, the IPR for a point-like return in one dimension is a $\sin(\pi x)/(\pi x)$ function as represented in Fig. 2(a). The function in Fig. 2(a) is also commonly referred to as a *sinc* function. The nearest sidelobe is -13.5 dB below the peak, and the sidelobe envelope decreases 6 dB per octave (for each additional factor-of-two distance from the origin) beyond that. Since SAR imagery can have a dynamic range (ratio of largest to smallest target) of 50 dB or higher, the *sinc* function sidelobes from a strong target can easily interfere or obscure nearby targets which have weaker return signal strength.

Sidelobes in SAR imagery have traditionally been reduced by applying an amplitude weighting function to the data prior to the final FFT, as illustrated in Fig. 1. An example is the Hanning weighting function which gives the impulse response shown in Fig. 2(b). The Hanning peak sidelobe is much smaller than for the *sinc* function, and the sidelobe envelope decreases at 18 dB per octave. However, the lower sidelobes have been achieved at the expense of the mainlobe

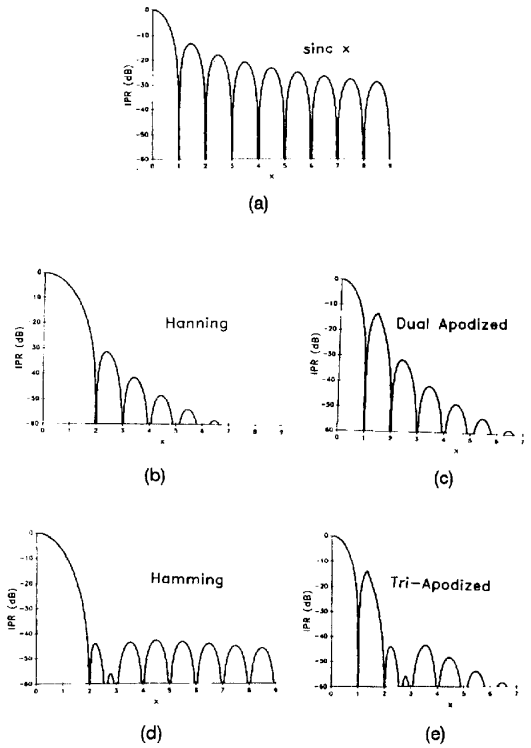

Fig. 2. IPRs. (a) Unweighted (sinc IPR). (b) With Hanning weighting. (c) Dual apodized. (d) With Hanning weighting. (e) Tri-apodized.

width which determines the ultimate resolution of the imagery. The Hanning mainlobe is twice as wide (null-to-null) as the *sinc* function. Many other weighting functions have been developed for a variety of purposes [2]. All, however, are a compromise between a narrow mainlobe (resolution) and low sidelobes.

Borrowing a term from optics, *apodization* [3] refers to the suppression of diffraction sidelobes. Weighting or shaping a finite aperture is the most conventional linear form of apodization, although nonlinear techniques are beginning to appear [5]. The shaping and shading of SAR data prior to the final Fourier transform for sidelobe control is completely analogous to sidelobe control for optics. Traditionally, SAR aperture weighting is applied in the Fourier domain, resulting in a spatially invariant IPR that is the same for every location in the image. The purpose of this work is to show that apodization can be accomplished on a pixel-by-pixel basis, using nonlinear operators, to suppress sidelobes while preserving the mainlobe resolution. The term apodization is used to distinguish these more general image-domain techniques from the conventional linear aperture weighting, which is but one method of apodization.

Part II describes the first step in the conceptual development of nonlinear apodization, i.e., dual and multiapodizations. Better sidelobe control is achieved by increasing the number of apodizations from which to choose. Parts III and IV complete the process by showing how a continuous family of aperture weightings can be utilized at each pixel to effectively null out the sidelobe energy, if it is present. Strategies for 2-D implementations are explored in Section V.

Part VI shows an example of these techniques applied to real SAR imagery, and Part VII summarizes the results and suggests other applications.

II. DUAL AND MULTIAPODIZATION

One nonlinear procedure for obtaining an image with good mainlobe resolution and low sidelobes is to do the following.

1) Compute two versions of the image, each having a different IPR, one using uniform weighting (resulting in the *sinc* IPR as shown in Fig. 2(a)), and a second one using a different weighting such as Hanning (the Hanning IPR is shown in Fig. 2(b)).

2) At each spatial location, select the minimum value from the pair of images.

We call this procedure dual apodization (DA).

If the scene consists of a single bright point, then the two versions of the image are the IPRs shown in Figs. 2(a) (*sinc*) and 2(b) (Hanning). The resultant dual-apodized IPR, shown in Fig. 2(c), has the narrow mainlobe of the *sinc* IPR and the small sidelobes of the Hanning IPR.

More generally, DA refers to the combination of a uniformly weighted image with a normalized version of the same image computed with any weighting function chosen to produce low sidelobes. The combination technique uses a *min* function applied to the detected image on a pixel-by-pixel basis.

Applied to complicated images, DA results in an effective weighting function that can differ from sample to sample in the image. Thus it results in a weighting function and an IPR that are both nonlinear and spatially varying.

If preservation of the original phase of the image is desired, then the second step for the DA procedure given above would become: 2) at each spatial location, select the complex value from the pair of images whose magnitude is minimum.

Tri-apodization is a logical extension of DA in which the output pixel value is selected from the minimum of 3 images processed with different weighting functions. Consider the Hamming [2] IPR given in Fig. 2(d), where the Hamming weighting function is designed to place a null in the second sidelobe of the *sinc* function (first sidelobe of the Hamming IPR). Taking the *min* of the *sinc*, Hanning, and Hamming IPRs of Figs. 2(a), 2(b), and 2(d) gives the tri-apodized IPR of Fig. 2(e).

It is easy to visualize further improvement via multiapodizations using even larger numbers of weighting functions.

III. COMPLEX DUAL APODIZATION

DA makes a decision based only on the magnitudes of the images; however, additional information resides in the complex values of the images. To make use of the complex values we operate on the real (I or in-phase) and imaginary (Q or quadrature) components of the undetected images separately. If the value of a component has a sign that is different for the *sinc* IPR than for the Hanning IPR, then there must be some weighting function intermediate between uniform weighting and Hanning weighting for which the value of the component would be zero. Making use of the sign change is a way to effectively make use of a family of IPRs while only having to compute two of them.

We call the following algorithm, which makes use of this principle, complex DA (CDA). 1) Compute two versions of the image, one using uniform weighting and the other using Hanning weighting, and then 2) at each spatial location, if the I components of the two images have opposite sign, select the value zero; otherwise select the I value which has the smaller absolute value of the two. Do likewise for the Q components.

CDA is especially powerful because the sidelobes for the two IPRs are opposite in sign. The result of CDA for a scene consisting of a single bright point would simply be the mainlobe of the *sinc* function in Fig. 2(a).

CDA provides significantly lower sidelobes than DA for the one-dimesional case (1-D). However, in a 2-D image the IPR changes sign only along the cardinal directions. For this case, CDA is less effective for sidelobes not along the cardinal directions than for those which lie along the cardinal axes.

IV. SPATIALLY VARIANT APODIZATION IN ONE DIMENSION

Both DA and CDA have dramatic positive impact on the visual appearance of SAR imagery which consists of many complex scatterers. Tri-, quad-, or higher order multiapodizations should yield further improvement but at the expense of an increased computational burden.

In this section we describe a more general algorithm, which we call spatially variant apodization (SVA), which allows each pixel in an image to receive its own frequency domain aperture amplitude weighting function from a continuum of possible weighting functions. SVA effectively eliminates finite-aperture induced sidelobes from uniformly weighted SAR data while retaining nearly all of the good mainlobe resolution and clutter texture of the unweighted SAR image, and is extremely simple computationally. This is accomplished by taking advantage of the special properties of raised-cosine weighting functions when dealing with sampled images. We first derive 1-D versions of the algorithm and show some of its properties. Later we give the 2-D version.

It is well known [2] that cosine-on-pedestal frequency domain weighting functions can be implemented using a 3-point convolver on complex, Nyquist-sampled imagery. The cosine-on-pedestal weighting functions are given by

$$A(n) = 1 + 2w\cos(2\pi n/N). \tag{1}$$

This family of weightings range from uniform weighting ($w = 0$: all pedestal, no cosine) to Hanning weighting ($w = 0.5$: all cosine, no pedestal). Hamming weighting is a special case of cosine-on-pedestal which nulls the first sidelobe ($w = 0.43$). Similarly, any unweighted aperture *sinc*-function sidelobe can be suppressed using one of the family of cosine-on-pedestal weighting functions.

Taking the length-N discrete Fourier transform of a cosine-on-pedestal weighting function yields the Nyquist-sampled IPR:

$$a(m) = w\delta_{m,-1} + \delta_{m,0} + w\delta_{m,1} \tag{2}$$

where $\delta_{m,n}$ is the Kronecker delta function,

$$\delta_{m,n} = \begin{cases} 1, & m = n \\ 0, & m \neq n \end{cases}. \tag{3}$$

The fact that this IPR contains only three non-zero points allows the imposition of any of this family of weighting functions to be efficiently performed by convolution in the image domain by the three-point kernel given in (2).

We consider two approaches: minimizing for I and Q jointly, which is the most natural extension of DA, and minimizing I and Q separately, which is computationally simpler and yields even greater sidelobe suppression in the presence of clutter.

I and Q Jointly: Let $g(m) = I(m) + iQ(m)$ be the complex-valued samples of a uniformly weighted Nyquist-sampled image. Using the 3-point convolver given in (2) to achieve a given cosine-on-pedestal aperture weighting, $g(m)$ is replaced by $g'(m)$ as follows:

$$g'(m) = w(m)g(m-1) + g(m) + w(m)g(m+1). \tag{4}$$

As $w(m)$ varies from 0 to 1/2, the frequency domain amplitude weighting varies from cosine-on-zero pedestal (Hanning) at $w(m) = 1/2$ to uniform weighting at $w(m) = 0$. The center convolver weight is always unity because, in the manner of DA, we wish to normalize the peaks of the point-target responses for the family of cosine-on-pedestal weightings.

The task, therefore, is to find the $w(m)$ which minimizes $|g'(m)|^2$ subject to the constraints $0 \leq w(m) \leq 1/2$. The unconstrained $w(m)$ that gives the minimum is obtained by setting equal to zero the partial derivative of $|g'(m)|^2$ with respect to $w(m)$, and solving for $w(m)$:

$$w_u(m) = -\mathrm{Re}\left[\frac{g(m)}{g(m-1)+g(m+1)}\right] \tag{5a}$$

$$= \frac{-|g(m)|}{|g(m-1)+g(m+1)|} \times \cos\{\arg[g(m)] - \arg[g(m-1)+g(m+1)]\} \tag{5b}$$

$$= -\frac{-\{I(m)[I(m-1)+I(m+1)] + Q(m)[Q(m-1)+Q(m+1)]\}}{[I(m-1)+I(m+1)]^2 + [Q(m-1)+Q(m+1)]^2} \tag{5c}$$

where $\arg[g]$ is the phase of g. We constrain $w(m)$ in (5) to be in the interval $[0,1/2]$ by letting $w(m) = 0$ for $w_u \leq 0$, $w(m) = w_u(m)$ for $0 < w_u(m) < 1/2$, and $w(m) = 1/2$ for $w_u(m) \geq 1/2$. Inserting this into (4) yields the output image

$$g'(m) = \begin{cases} g(m), & w_u(m) < 0 \quad (6a) \\ g(m) + w_u(m)[g(m-1)+g(m+1)], & 0 \leq w_u(m) \leq 1/2 \quad (6b) \\ g(m) + (1/2)[g(m-1)+g(m+1)], & w_u > 1/2. \quad (6c) \end{cases}$$

Equation (6a), $g'(m) = g(m)$, is in force where $w_u(m) < 0$. From (5b) we see that this occurs where the phases of $g(m)$ and $[g(m-1)+g(m+1)]$ are within $\pi/2$ of one another. This condition holds for a sample near a peak of an IPR, and so impulse-response peaks are preserved.

Where the phases of $g(m)$ and $[g(m-1)+g(m+1)]$ differ by more than $\pi/2$, $w_u(m) > 0$ and (6b) or (6c) is in force. Equation (6b) can be written as

$$g'(m) = g(m)[\tfrac{1}{2} - \tfrac{1}{2}\exp\{i2\arg[g(m-1)+g(m+1)] - i2\arg[g(m)]\}]. \tag{7}$$

From this expression we see that where the difference between the phases of $g(m)$ and $[g(m-1)+g(m+1)]$ approaches π, $g'(m)$ approaches zero. Since sidelobes change phase by π from one Nyquist sample to the next, this condition holds for a sample in a sidelobe region, and so sidelobes are suppressed. Where the phases of $g(m)$ and $[g(m-1)+g(m+1)]$ differ by less than π, the suppression is less complete. Where the phases differ by $\pi/2$ or less, $g'(m) = g(m)$ and the value is preserved.

I and Q Separately: Now let $g(m)$ be the samples of either the real (I) or imaginary (Q) component of a uniformly weighted Nyquist-sampled image. The output from the 3-point convolver to achieve a given cosine-on-pedestal aperture weighting is again given by (4), but with the new interpretation of $g(m)$ as being a real-valued component. Solving for $w_u(m)$ that minimizes $[g'(m)]^2$, we obtain the unconstrained $w(m)$ that gives the minimum:

$$w_u(m) = \frac{-g(m)}{g(m-1)+g(m+1)}. \tag{8}$$

This can also be gotten by directly solving for $g'(m) = 0$.

If $w_u(m)$ in (8) is inserted into (4), then we get $g'(m) = 0$. Constraining $w_u(m)$ in (8) to lie in the interval $[0, \frac{1}{2}]$, and inserting it into (4) yields the output image:

$$g'(m) = \begin{cases} g(m), & w_u(m) < 0 \quad (9a) \\ 0, & 0 \leq w_u(m) \leq 1/2 \quad (9b) \\ g(m) + (1/2)[g(m-1)+g(m+1)], & w_u(m) > 1/2. \quad (9c) \end{cases}$$

Therefore, wherever $0 \leq w_u(m) \leq 1/2$, we have $g'(m) = 0$; but $g'(m)$ can be non-zero wherever $w_u(m) < 0$ or $w_u(m) > 1/2$. Equation (9) is performed on the I and Q values independently.

The result is a minimization of the I^2 and Q^2 pixel values independently for an infinite but bounded set of frequency-domain weighting functions chosen from the cosine-on-pedestal family.

We denote the average of the two nearest neighbors to $g(m)$ as

$$y = (1/2)[g(m-1)+g(m+1)]. \tag{10}$$

Fig. 3(a) shows the constrained w as a function of $g(m)/y$, and Fig. 3(b) shows the output image value, $g'(m)$, normalized by y, as a function of $g(m)/y$. Region I shown in the figure represents 9(a), which assumes that $g(m)$ is within a mainlobe, since $g(m)$ and y have the same sign. Then $w = 0$ and $g'(m) = g(m)$, i.e., the mainlobe areas are preserved. Region II represents 9(b), which assumes that $g(m)$ is within an area of pure sidelobes, since $g(m)$ and y have opposite signs and $|g(m)| < |y|$. Then $0 < w < 1/2$ and $g'(m) = 0$, i.e., the sidelobe areas are completely suppressed. Region III represents 9(c), which assumes that $g(m)$ is in a region of a mainlobe superimposed with sidelobes, since $g(m)$ and y have opposite signs and $|g(m)| > |y|$. Then $w = 1/2$ and $g'(m) = g(m) + y$. From Fig. 3(b) we see that in Region III $|g'(m)| \leq |g(m)|$, i.e., the image is suppressed somewhat in an attempt to reduce the influence of the sidelobes.

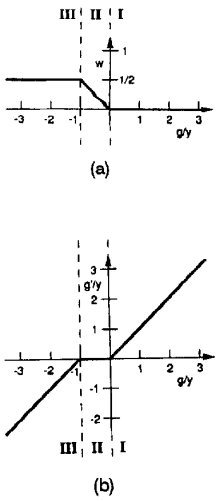

Fig. 3. SVA operating regions.

From these considerations we can also see that I,Q-separately SVA can be expressed by

$$\text{If} \quad g(m)y \geq 0, \quad \text{then} \quad g'(m) = g(m) \tag{11a}$$

$$\text{else if} \quad |g(m)| < |y|, \quad \text{then} \quad g'(m) = 0 \tag{11b}$$

$$\text{otherwise} \quad g'(m) = g(m) + y. \tag{11c}$$

Here we have used the fact that $g(m)y \geq 0$ implies that $g(m)$ and y have the same sign. Equations (10) and (11) represent a compact, efficient implementation of SVA.

Relationship Between 1-D CDA and I,Q-Separately SVA: For Nyquist-sampled imagery, in one dimension, CDA using Hanning weighting can be expressed as

$$g_h(m) = (\tfrac{1}{2})g(m-1) + g(m) + (\tfrac{1}{2})g(m+1) \tag{12}$$

$$\text{if} \quad g(m)g_h(m) \leq 0, \quad \text{then} \quad g'(m) = 0 \tag{13a}$$

$$\text{else if} \quad |g(m)| < |g_h(m)|, \quad \text{then} \quad g'(m) = g(m) \tag{13b}$$

$$\text{else} \quad g'(m) = g_h(m). \tag{13c}$$

We show in Appendix A that this version of CDA and I,Q-separately SVA are equivalent. However, as seen later, when operating in both dimensions simultaneously, they are not equivalent.

Integer Nyquist Sample Rates: Twice-Nyquist, or other integer-Nyquist image sample rates, are easily handled by simply applying (4) with (5) or (8) to pixels m, $m-k$ and $m+k$ for an image sample rate k times Nyquist.

Noninteger Nyquist Sample Rates: We have found that the SVA algorithm is robust with respect to sample rates other than an integer multiple of Nyquist. For example, good results are obtained if the maximum weight constraint of $\frac{1}{2}$ is increased to 0.6 for sample rates up to 20 percent greater or less than k-time-Nyquist.

Smoothing and Final DA: Some smoothing may be desirable for the I and Q image components to improve clutter appearance after either SVA or CDA are applied. In clutter areas, SVA and CDA introduce zeros and lower valued pixels which distort the original clutter histogram. Smoothing tends to restore the clutter histogram, albeit at the expense of some clutter correlation and point target spreading. B. Thelen at ERIM has studied extensively the effects of SVA on clutter and histogram restoration by smoothing. His results are documented in internal memos which will be the basis for a future work.

The spreading of point targets with smoothing can be mostly eliminated by performing DA of the smoothed, detected SVA image with the detected original unweighted image. The example image in Section VI was produced using $I-Q$ independently SVA followed by smoothing of the I and Q components and final DA of the real-valued detected images.

Algorithm Analysis for a Single Sinc Function: We now analyze some specific cases for 1-D SVA, starting with the simplest: an object consisting of a single delta function. Suppose that we begin with a uniform-weighted aperture, for which the coherent impulse response is

$$c(x) = \operatorname{sinc}(x) = \frac{\sin \pi x}{\pi x}. \tag{14}$$

Let the object be a single delta function at location x_0:

$$f(x) = \delta(x - x_0) \tag{15}$$

for which the image is the convolution of $c(x)$ with $f(x)$, i.e.,

$$g(x) = c(x) * f(x) \tag{16}$$

of which we have only the samples

$$g(m) = \operatorname{sinc}(m - x_0) = \frac{\sin \pi(m - x_0)}{\pi(m - x_0)} \tag{17}$$

where m is an integer sample number. Using the identity

$$\sin \pi(m - x_0 \pm 1) = -\sin \pi(m - x_0) \tag{18}$$

we have

$$g(m \pm 1) = \frac{-\sin \pi(m - x_0)}{\pi(m - x_0 \pm 1)} \tag{19}$$

and more generally, for any integer p,

$$g(m \pm (2p+1)) = \frac{-\sin \pi(m - x_0)}{\pi(m - x_0 \pm (2p+1))} \tag{20}$$

and

$$g(m \pm 2p) = \frac{\sin \pi(m - x_0)}{\pi(m - x_0 \pm 2p)}. \tag{21}$$

That is, the numerator is the same at all samples, except for an alternating factor of ± 1. Inserting (19)

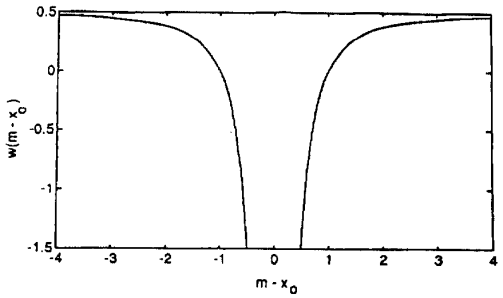

Fig. 4. SVA weight for single sinc function.

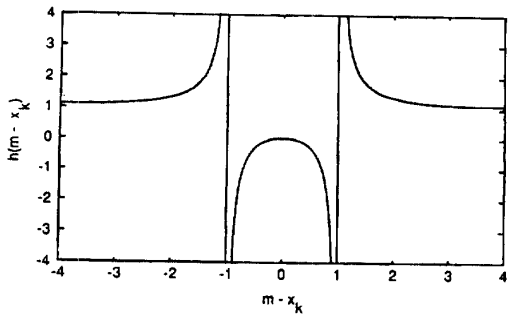

Fig. 5. $h(m-x_k)$ versus $(m-x_k)$.

into (8) and simplifying yields

$$w_0(m) = \frac{-\text{sinc}(m-x_0)}{\text{sinc}(m-1-x_0)+\text{sinc}(m+1-x_0)} = \frac{\dfrac{1}{m-x_0}}{\dfrac{1}{m-1-x_0}+\dfrac{1}{m+1-x_0}} = \frac{(m-x_0)^2-1}{2(m-x_0)^2} \tag{22}$$

which is plotted in Fig. 4.

The pertinent properties of $w_0(m)$ are as follows:

$$\lim_{|m-x_0|\to\infty} w_0(m-x_0) = 0.5 \tag{23a}$$

$$w_0(\pm 1) = 0 \tag{23b}$$

$$w_0(0) = -\infty. \tag{23c}$$

Since, as noted earlier, $g'(m) = 0$ wherever $0 \le w_0(m) \le 1/2$, and since $w_0(m-x_0)$ lies between 0 and 1/2 for $1 \le |m-x_0| \le \infty$, we find that all the sidelobes of this single *sinc* function are made exactly zero by SVA.

For the Nyquist-sampled image assumed here, the mainlobe of the *sinc* function consists of a single point if x_0 is an integer, and a pair of points if x_0 is not an integer. For x_0 an integer, $g(x \pm 1) = 0$ and from (4) we see that $g'(x_0) = g(x_0)$, and the mainlobe is unaffected by the algorithm. For x_0 not an integer, let m_0 be the sample immediately to the left of x_0. Then the mainlobe consists of the two samples m_0 and (m_0+1), and from Fig. 4 we see that $w_0(m_0)$ and $w_0(m_0+1)$ are both less than 0 since $|m_0 - x_0| < 1$ and $|m_0 + 1 - x_0| < 1$. Consequently, in the algorithm $w_0(m_0)$ and $w_0(m_0+1)$ are truncated to zero. Therefore, $g'(m_0) = g(m_0)$ and $g'(m_0+1) = g(m_0+1)$, i.e., the mainlobe is unaffected by the algorithm. Therefore, for the case of a single *sinc* function, the algorithm is perfect in that it exactly preserves the *sinc* mainlobe while exactly eliminating all the sidelobes.

One way to see how the algorithm works is to note that in the sidelobe region $g(m)$ oscillates between positive and negative values, has an amplitude that is decreasing montonically away from the peak, and has a positive second derivative. This makes $g(m-1)+g(m+1)$ in the denominator of (8) always of opposite sign but slightly greater in magnitude than twice $g(m)$ in the numerator. This makes $w_0(m)$ slightly less than 1/2, putting it in the interval [0,1/2] where $g'(m) = 0$, wiping out the sidelobes. In the mainlobe region, however, either $g(m-1)$ or $g(m+1)$ will have the same sign as $g(m)$, and the one with the same sign will be larger in magnitude than the one with opposite sign. Therefore, $w_0(m)$ by (8) will be negative in the mainlobe, and the algorithm then truncates $w_0(m)$ to zero, making $g'(m) = g(m)$, preserving the mainlobe. From this we see that the algorithm suppresses oscillatory regions of nearly uniform magnitude, characteristic of sidelobes, while preserving local maxima and regions where the sign does not oscillate at every pixel, characteristic of mainlobes.

Multiple Sinc Case: We now analyze an object consisting of a collection of delta functions:

$$f(x) = \sum_{k=1}^{K} a_k \delta(x - x_k) \tag{24}$$

for which the image at the sample points is

$$g(m) = \sum_{k=1}^{K} a_k \,\text{sinc}(m - x_k). \tag{25}$$

We are considering the case of I,Q-separately, so here the a_k are real-valued constants.

From (8), we have

$$w(m) = \frac{-\sum_{k=1}^{K} a_k \,\text{sinc}(m-x_k)}{\sum_{k=1}^{K} a_k \,\text{sinc}(m-1-x_k)+\sum_{k=1}^{K} a_k \,\text{sinc}(m+1-x_k)} = \frac{\sum_{k=1}^{K} a_k \,\text{sinc}(m-x_k)}{2\sum_{k=1}^{K} a_k \,\text{sinc}(m-x_k)\dfrac{(m-x_k)^2}{(m-x_k)^2-1}}. \tag{26}$$

Of particular interest is the factor

$$h(m,x_k) = \frac{(m-x_k)^2}{(m-x_k)^2-1} \tag{27}$$

which is plotted in Fig. 5. We see that for a single *sinc*, $h(m,x_k)$ is $0.5/w_0(m)$ (see (22) and Fig. 4). From the

plot in Fig. 5, we see that $h(m,x_k)$ is slightly greater than 1 for large $|m-x_k|$. Therefore, for samples far away from the mainlobes of all the *sinc* functions (that is, for $|m-x_k|>3$ for all k), this factor is nearly a constant, and the denominator in the equation for $w(m)$ above will be approximately twice as large as the numerator, and we will have $w(m)$ slightly less than 1/2. For those samples $g'(m)=0$ and the sidelobes are completely suppressed.

However, further analysis of SVA reveals there are some special circumstances where the sidelobes are not perfectly suppressed for *any* cosine-on-pedestal weighting for which $0 \le w(m) \le 0.5$. In particular, suppose that the factors $(m-x_k)^2/[(m-x_k)^2-1]$ in the denominator of the equation above are such that the terms in the denominator exactly or almost exactly cancel, making the denominator zero or nearly zero. Then the terms in the numerator, which are the same as those in the denominator but without the factors, may not cancel as well, and we could have $w(m)>1/2$ even for points away from the mainlobes.

In order to understand this situation further, consider the case of two *sinc* functions, where we model

$$g(m) = \mathrm{sinc}(m-x_1) + a\,\mathrm{sinc}(m-x_2) \tag{28}$$

which is the multiple-sinc case with $a_1=1$ and $a_2=a$. Then

$$w(m) = \frac{\mathrm{sinc}(m-x_1)+a\,\mathrm{sinc}(m-x_2)}{2[\mathrm{sinc}(m-x_1)h(m,x_1)+a\,\mathrm{sinc}(m-x_2)h(m,x_2)]}. \tag{29}$$

Suppose that x_1 is not an integer and let

$$b = a\,\mathrm{sinc}(m-x_2)/\mathrm{sinc}(m-x_1). \tag{30}$$

Then we can rewrite $w(m)$ as (for $b>0$),

$$w(m) = \frac{1+b}{2[h(m,x_1)+bh(m,x_2)]}, \tag{31}$$

$$1+b < h(m,x_1)+bh(m,x_2) \tag{32}$$

since outside the mainlobes $h>1$. We then have $0<w(m)<1/2$ yielding $g'(m)=0$ and the sidelobes are completely suppressed. This happens whenever the two sidelobes, $\mathrm{sinc}(m-x_1)$ and $a\,\mathrm{sinc}(m-x_2)$ have the same sign at sample m. However, if the sidelobes have opposite signs, then this guarantee of sidelobe suppression does not hold.

A strategy for finding a case where a sidelobe far from the mainlobe is not completely suppressed is to pick parameters such that the denominator in the equation above for $w(m)$ is near zero, yet the numerator is not. This requires that $h(m,x_1)$ and $h(m,x_2)$ have substantially different values. For example, consider the case of $x_1=0.5$, $x_2=10.5$, and $m=4$. We have $h(4,0.5)=1.0889$ and $h(4,10.5)=1.02424$, which have a ratio of 0.94063. If we choose a so that $b=-1/0.9400$, then $w(4)=-0.0638/(-0.001434)=44.5$. In this case the sidelobe at $m=4$ will not be reduced at all, even though it is 3.5 Nyquist samples from the nearest mainlobe peak. Note, however, that to contrive this case it was necessary to have sidelobes that were nearly canceling one another anyway. The sidelobes from the two sinc functions largely canceled one another, having a combined relative value of $1-1/0.94=-0.0638$, which is about 24 dB down from the value of an individual sinc sidelobe. Therefore, while this behavior constitutes an exception to perfect cancellation, it does not represent a severe case of failure. In fact, it shows that there simply is *no* cosine-on-pedestal weighting function between uniform and Hanning which will reduce this sidelobe any further.

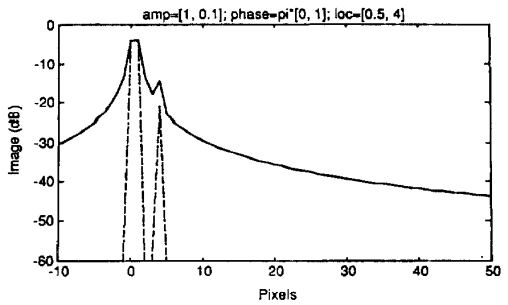

Fig. 6. SVA operating on 2 delta functions giving ideal sidelobe suppression. Solid line: original Nyquist-sampled image; dashed line: I,Q-separately SVA; dotted line: $I-Q$-jointly SVA (the latter two curves overlap).

The behavior of the algorithm was also studied using simulations in which the algorithm was applied to sums of sinc functions with various amplitudes, phases, and locations. For most cases the algorithm worked perfectly, completely suppressing the sidelobes while retaining the mainlobe. There were, however, a few cases in which it seemingly did not work perfectly, as would be expected from the analysis presented above.

Fig. 6 shows an example of a typical case in which it worked perfectly. The sum of two sincs separated by 3.5 samples, with a peak ratio of 0.5, and a relative phase of pi radians is shown in the upper solid line which is drawn to connect adjacent Nyquist samples. The vertical scale is in dB. In the figure the output of I,Q-separately SVA is shown in dashed lines and that of I,Q-jointly SVA is shown in dotted lines. The amplitudes, phases, and locations of the sinc functions are listed just above the plot. In this instance the two versions of SVA gave the identical result and those two curves are superimposed.

Fig. 7 shows the example discussed above in which a single sidelobe was not cancelled. Recall that a was chosen so that $b=-1/0.94$. Then we have $a=b\,\mathrm{sinc}(4-0.5)/\mathrm{sinc}(4-10.5)=1.9757$. Note that the sidelobe at the minimum between the two peaks at $m=4$ is not suppressed, although all the other sidelobes are completely suppressed. Again,

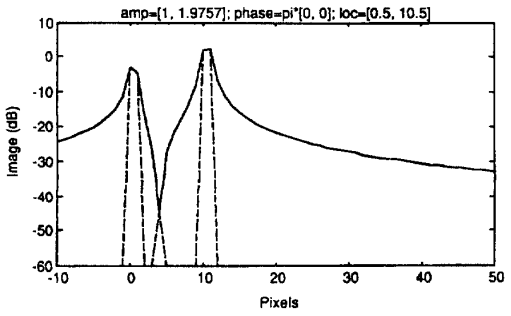

Fig. 7. SVA operating on 2 delta functions with nonideal sidelobe suppression (see text).

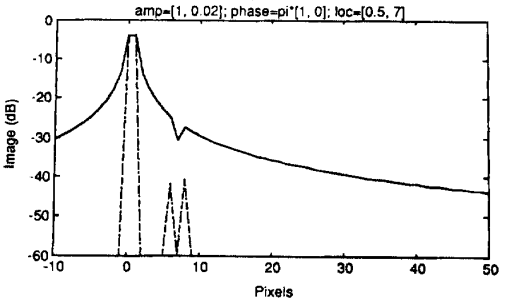

Fig. 8. SVA operating on 2 delta functions resulting in split second peak.

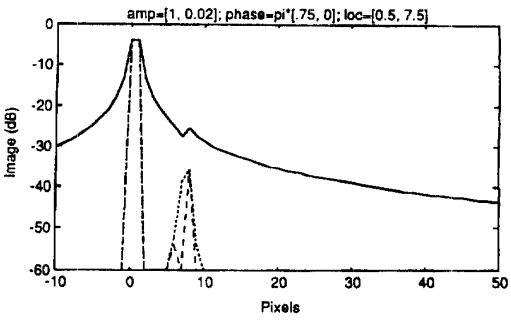

Fig. 9. SVA operating on 2 delta functions with only I,Q-separately SVA splitting second peak.

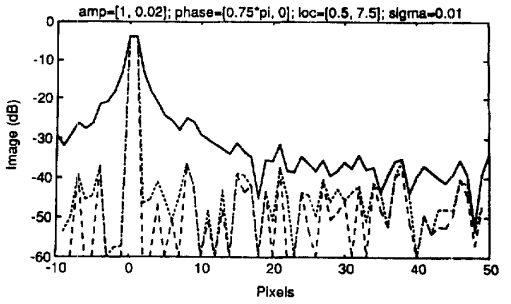

Fig. 10. SVA with -40 dB noise added.

the behavior illustrated in Fig. 7 is not an added artifact of the algorithm, it simply indicates that no cosine-on-pedestal weighting function between uniform and Hanning can reduce the remaining sidelobe any further. However, SVA eliminates many more sidelobes than any single cosine-on-pedestal weighting could, and without increasing the mainlobe widths.

Fig. 8 shows an example of another behavior observed. In this case a single peak (at sample 7) is split into a pair of peaks (at samples 6 and 8), with a null at the position of the true peak of the second sinc. Both versions of the algorithm gave the same result. Split-peak responses also occurs for any single cosine-on-pedestal weighting where a sidelobe from a strong target interferes with a weaker target which is comparable in amplitude to the sidelobe but of opposite phase. This behavior is, therefore, not peculiar to the SVA algorithm; however, SVA greatly improves the detectability of the weaker target compared with any single cosine-on-pedestal weighting by suppressing the nearby sidelobes.

The two versions of the algorithm did not always give identical results. Keeping the same parameters as the previous example, changing only the phase of the second peak from π to $3\pi/4$, gives the result in Fig. 9. The I,Q-separately algorithm yields an asymmetric pair of peaks at $m = 6$ and 8, while the I,Q-jointly algorithm yields a single broader peak. Which result is preferable may depend on the application. There are other cases in which the I,Q-jointly algorithm yields a broader peak for which the I,Q-separately algorithm yields only a single substantial peak; in these cases the I,Q-separately algorithm is superior to the I,Q-jointly algorithm.

Effects of Noise on SVA: The effects of noise on the algorithm are demonstrated by adding zero-mean Gaussian noise to the image prior to performing the algorithm. An example is shown in Fig. 10 in which the parameters were the same as the previous example, but noise with an rms value of 0.01 (-40 dB) was added to the complex values prior to applying the algorithm. We see that where the sidelobes are above the noise level, the algorithm reduces the sidelobes down to the noise level. Sidelobes that are dominated by noise are not reduced much; this is expected since the algorithm is designed to reduce sidelobes, not to reduce noise. From these results we also see that the algorithm is not very sensitive to noise: the presence of the noise does not prevent the algorithm from reducing the sidelobes down to the level of the noise.

Effect of Phase Errors on SVA: SVA provides partial reduction of the effects of phase errors (even though it was not designed to do so); sinusoidally varying sidelobes away from the main smear are still suppressed by SVA despite the presence of phase errors. This is demonstrated by the example shown in Fig. 11, which shows SVA for an object consisting of two delta functions and the phase error is one wave center-to-edge of quadratic. Artifacts at the left and

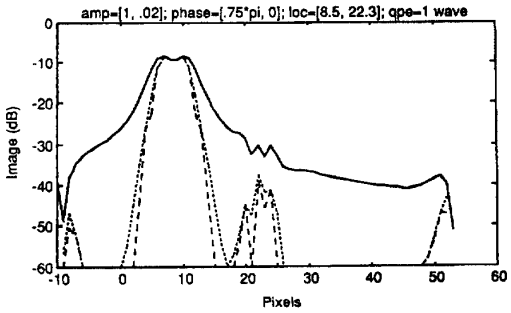

Fig. 11. SVA with phase errors.

right edges of the plots should be ignored since they involve aliasing effects of the simulation.

The narrowing of the mainlobe of the IPR with SVA is noticeable but modest. One way of understanding the improvement is as follows. The more severe cosine-on-pedestal weightings significantly weight down the edges of the aperture. This reduces the effects of the phase error, since it is at the edges of the aperture that the slope of the phase error is most severe.

In areas in-between the mainlobes of the two smeared sinc functions (for the smaller phase errors for which the two mainlobes do not merge) and in the areas away from both mainlobes, the SVA algorithm remains effective in suppressing the sidelobes, despite the phase errors, as seen in Fig. 11.

V. SVA IN TWO DIMENSIONS

Two Dimensions Sequentially: When implementing SVA in two dimensions, one approach is to perform the 1-D algorithm in each of the dimensions sequentially, that is, to perform 1-D SVA first along the horizontal direction and then on that result perform 1-D SVA along the vertical direction. This approach is fast and performs well, but has the disadvantage that the second application of the algorithm in the vertical direction is not operating on a properly Nyquist-sampled image. Unlike CDA, SVA performed sequentially will eliminate all sidelobes for a single point scatterer including those which are not along the cardinal axes.

Two Dimensions Simultaneously: As before, we consider both the I,Q-separately and the I,Q-jointly cases. Furthermore, we can have the two dimensions either coupled or uncoupled.

We employ the family of 2-D impulse responses with samples

$$\begin{pmatrix} w_m w_n & w_n & w_m w_n \\ w_m & 1 & w_m \\ w_m w_n & w_n & w_m w_n \end{pmatrix}$$

where w_m and w_n are the weighting factors in the m and n directions that arise from a family of Nyquist-sampled separable raised-cosine weighting functions. Both w_m and w_n depend on (m,n). By allowing $w_m \neq w_n$, the two dimensions can be uncoupled. Let

$$Q_m = g(m-1,n) + g(m+1,n) \tag{33}$$

$$Q_n = g(m,n-1) + g(m,n+1) \tag{34}$$

and

$$P = g(m-1,n-1) + g(m+1,n+1) + g(m-1,n+1) + g(m+1,n-1). \tag{35}$$

Then at pixel (m,n) the convolution of the IPR, described in matrix form above, with the image is given by

$$g'(m,n) = g(m,n) + w_m w_n P + w_m Q_m + w_n Q_n. \tag{36}$$

The SVA algorithm would be to minimize $|g'(m,n)|^2$ as a function of (w_m, w_n), subject to $0 \leq \{w_m, w_n\} \leq \frac{1}{2}$.

I,Q-Separately, Two Dimensions Coupled: First consider the case of $w_m = w_n = w$, for which the weightings in the two dimensions are coupled, and I and Q separately, for which $g(m,n)$ is either the I or Q component of the image. Then we have

$$g'(m,n) = g(m,n) + w^2 P + wQ \tag{37}$$

which has zeros at

$$w_0 = \frac{-Q \pm \sqrt{Q^2 - 4Pg(m,n)}}{2P} \tag{38}$$

where

$$Q = Q_m + Q_n = g(m,n-1) + g(m,n+1) + g(m-1,n) + g(m+1,n). \tag{39}$$

If $[Q^2 - 4Pg(m,n)] < 0$, then w_0 is complex-valued, and $g'(m,n)$ has no zeros. Now, $g'^2(m,n)$ has local extrema at the values of w for which $0 = \partial g'^2(m,n)/\partial w$, which are given by the two values of w_0 given above and by

$$w_e = \frac{-Q}{2P}. \tag{40}$$

When w_0 is complex valued, $g'^2(m,n)$ has only a single local extremum, at w_e.

In order to accommodate all possibilities, a logical SVA algorithm would be as follows, for this case of I,Q-separately, and the two dimensions simultaneously and coupled.

1) Compute w_0 (two values). If the w_0 are real valued and if either of the w_0 lies in the interval $[0,1/2]$, then $g'(m,n) = 0$.

2) Otherwise, compute w_e and compute $g'(m,n)$ for the three values of $w = \{0, 1/2, w_e\}$, and select the $g'(m,n)$ that has the minimum magnitude.

When the two dimensions are coupled, then CDA is not equivalent to SVA. In particular, because the equation for $g'(m)$ above is quadratic in w, it is possible, for example, for $g'(m)$ to be positive for both $w = 0$ and $w = 1/2$ and have its minimum for a value of w between 0 and 1/2. Then CDA would yield a $g'(m)$ that is larger than the minimum, and SVA would be superior.

I,Q-Separately, Two Dimensions Uncoupled: Next consider the case in which we allow w_m and w_n to differ, i.e., in which the two dimensions are uncoupled. First note that

$$\begin{aligned} g'(m,n) &= g(m,n) + w_m w_n P + w_m Q_m + w_n Q_n \\ &= g(m,n) + (w_n P + Q_m) w_m + w_n Q_n \end{aligned} \quad (41)$$

is, for any given w_n, a linear function of w_m. Similarly, for any given w_m, $g'(m,n)$ is a linear function of w_n. It follows that for any (w_m, w_n) interior to the box $[0,1/2] \times [0,1/2]$, the value of $g'(m,n)$ for either $(w_m,0)$ or $(w_m,1/2)$ will be less than or equal to the value for (w_m,w_n). Similarly, the value of $g'(m,n)$ for either $(0,0)$ or $(0,1/2)$ will be less than or equal to the value for $(w_m,0)$. By similar arguments, we see that both the maximum and minimum of $g'(m,n)$ are at the four corners of the box: at $(w_m,w_n) = (0,0)$, $(0,1/2)$, $(1/2,0)$, or $(1/2,1/2)$. Therefore for SVA it is necessary to check only those four values of (w_m,w_n). Furthermore, since $g'(m,n)$ is monotonic in w_m and w_n, it goes through zero within an interval if and only if it changes sign within the interval. Therefore checking the four corners by an extension of the CDA algorithm is equivalent to SVA for this case. Then a logical set of steps to perform SVA/CDA for the case of treating I,Q-separately, and the two dimensions simultaneously and uncoupled, would be as follows.

1) Compute $g'(m,n)$ for $(w_m,w_n) = (0,1/2)$, $(1/2,0)$, and $(1/2,1/2)$. If any of the three have sign opposite that of $g(m,n)$, then set $g'(m,n) = 0$.

2) Otherwise, for the four values of (w_m,w_n), select the $g'(m,n)$ that has the minimum magnitude.

Note that forcing $w_m = w_n = w$ (having the same weighting in both dimensions) will often leave higher sidelobes than the more general procedure described above. It is possible that $g'(m,n)$ will have a sign-change at $(w_m,w_n) = (0,1/2)$ or $(1/2,0)$ without going through zero along the line $w_m = w_n$ (or have a minimum at one of those two corners lower than the minimum along $w_m = w_n$). That is, for the case of I,Q-separately and the two dimensions simultaneously, uncoupling the two dimensions (i.e., allowing $w_m \neq w_n$) will give better sidelobe suppression than coupling them.

This method of handling the two dimensions simultaneously is preferable to handling two dimensions serially in that it avoids the problem for the serial case of the second dimension not being band limited when SVA is applied to it.

I,Q-Jointly: Treating I and Q jointly, the SVA algorithm would again be to minimize $|g'(m,n)|^2$ subject to $0 \leq \{w_m,w_n\} \leq 1/2$, but now g is taken to be the complex values of the image pixel, rather than just an I or Q component. When we do this, whether treating the two dimensions as either coupled or uncoupled, we are forced to solve an equation that is cubic in w. Since this version of the algorithm is considerably more complicated than the others, we omit the details here and recommend that, when treating the two dimensions simultaneously, for simplicity use the I,Q-separately version of the algorithm described above.

Minimum of Two 1-D: Another case to consider is a version of handling the two dimensions simultaneously, in which we employ the 1-D algorithms for each of the two dimensions independently and in parallel, and the minimum of those two results is used. Let us refer to this version as the "minimum-of-two-1-D." We can express the I,Q-separately, minimum-of-two-1-D version of SVA/CDA as follows.

1) Compute $g'(m,n)$ for $(w_m,w_n) = (0,1/2)$ and $(1/2,0)$. If either of the two have sign opposite that of $g(m,n)$, then set $g'(m,n) = 0$.

2) Otherwise, for the three values of (w_m,w_n), select the $g'(m,n)$ that has the minimum magnitude.

Note that this version of the algorithm is similar to the version of SVA treating I,Q-separately and two dimensions simultaneously and uncoupled, but ignoring the value of $g'(m,n)$ at $(w_m,w_n) = (1/2,1/2)$. Therefore it should be less effective in suppressing sidelobes.

For the versions investigated, the best 2-D implementation of SVA, from the point of view of suppressing sidelobes while being computationally efficient, seems to be version treating I,Q-separately, two dimensions simultaneously and uncoupled.

VI. IMAGE EXAMPLE

Fig. 12 shows SVA applied to a 1 m resolution SAR image collected by the ERIM Data Collection System (DCS) which is installed in a CV-580 aircraft. The scene contains two commercial ships berthed near Toledo, OH.

The top image (a) was processed using uniform weighting, while the bottom image (c) used a low-sidelobe, −30 dB Taylor weighting. The middle image (b) was processed using I,Q-separately SVA. The sample rate is twice-Nyquist in all three cases. A 3-point smoother (0.165, 0.770, 0.165) was applied to the I and Q pixels of the complex SVA image just prior to detection. In addition, a final dual apodization of the smoothed, detected, SVA image with the original

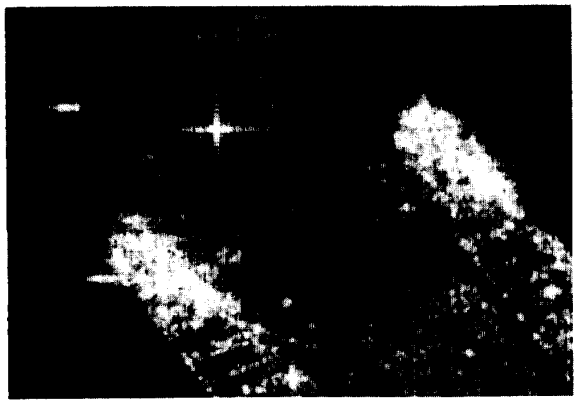

(a)

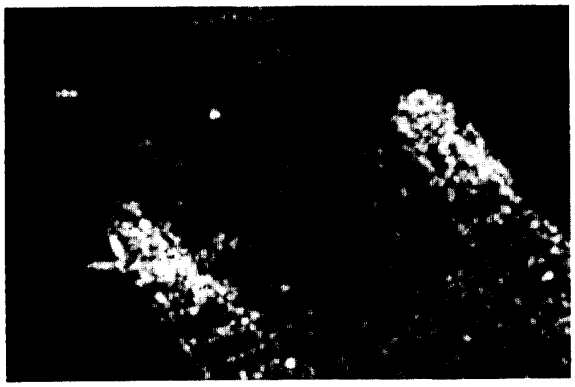

(b)

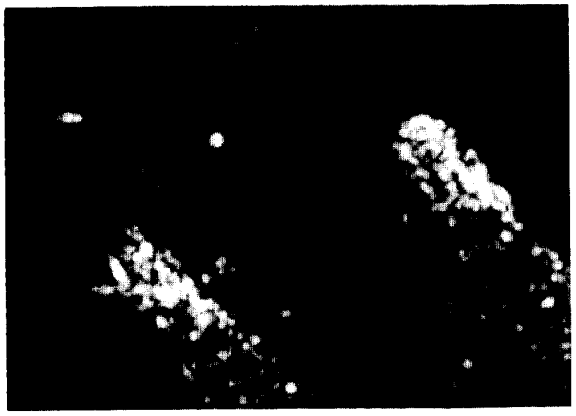

(c)

Fig. 12. SAR images demonstrating SVA. (a) Unweighted aperture. (b) SVA. (c) −30 dB Taylor weighting.

uniformly weighted image was undertaken to restore some of the sharpness lost in the smoothing.

Note that the SVA image preserves the fine resolution of the top image, yet has no visible sidelobes. Also note the preservation of the background clutter. It is of particular importance that nonlinear apodization techniques preserve clutter detail and texture for non-point-like areas in the image. Close examination reveals that the SVA image preserves the clutter speckle patterns of the original, uniformly weighted image better than the Taylor weighted image. As previously mentioned, the effects of SVA on clutter have been studied extensively, and will be the subject of a future work.

VII. SUMMARY AND CONCLUSIONS

Nonlinear apodization techniques have been introduced which reduce sidelobes in SAR imagery without sacrificing mainlobe resolution. DA works with detected, real-valued imagery. CDA and SVA are closely related techniques which operate on complex imagery to give much greater sidelobe suppression than DA. These techniques have potentially broad and far ranging applications in other fields as well; e.g. sonar, phased array antennas, radio astronomy, medical imaging (ultrasound, MRI, CAT), digital filtering, etc. The potential exists for application of these techniques wherever data can be represented as the Fourier transform of a finite aperture signal.

APPENDIX A

In this Appendix we show that in one dimension CDA using Hanning weighting and I,Q-separately SVA are equivalent. Recall that for CDA, $g'(m) = 0$ when the (I or Q) component for uniform weighting, $g(m)$, has sign opposite that for the Hanning-weighted image, $g(m) + (1/2)[g(m-1) + g(m+1)]$. Then

$$g(m)\{g(m) + (1/2)[g(m-1) + g(m+1)]\} < 0 \tag{42}$$

or

$$\begin{aligned} &g^2(m) + (1/2)g(m)[g(m-1) + g(m+1)] < 0, \\ &1 + \frac{[g(m-1) + g(m+1)]}{2g(m)} < 0 \\ &1 - \frac{1}{2w_u(m)} < 0 \\ &1 < \frac{1}{2w_u(m)} \end{aligned} \tag{43}$$

and

$$0 < w_u(m) < 1/2 \tag{44}$$

where $w_u(m)$ is given by (8). From (9b) we see that for this same condition, $g'(m) = 0$ for I,Q-separately SVA as well.

Recall that for CDA, when the signs of $g(m)$ and $g(m) + (1/2)[g(m-1) + g(m+1)]$ are the same, then the one with the minimum magnitude is chosen. Then,

similar to the derivation of (43),

$$g(m)\{g(m)+(1/2)[g(m-1)+g(m+1)]\}\geq 0 \tag{45}$$

$$1\geq \frac{1}{2w_u(m)} \tag{46}$$

and

$$w_u(m)\leq 0 \quad \text{or} \quad w_u(m)\geq 1/2. \tag{47}$$

If $w_u(m)\leq 0$, then

$$\begin{aligned}&\{g(m+(1/2)[g(m-1)+g(m+1)]\}^2\\ &\quad = g^2(m)\left[1-\frac{1}{2w_u(m)}\right]^2\\ &\quad \geq g^2(m)\end{aligned} \tag{48}$$

and CDA would choose $g'(m)=g(m)$; and according to (9a), I,Q-separately SVA would do the same. If $w_u(m)\geq 1/2$, then

$$0\leq \left[1-\frac{1}{2w_u(m)}\right]\leq 1 \tag{49}$$

and

$$\begin{aligned}&\{g(m)+(1/2)[g(m-1)+g(m+1)]\}^2\\ &\quad = g^2(m)\left[1-\frac{1}{2w_u(m)}\right]^2\\ &\quad \leq g^2(m)\end{aligned}$$

and CDA would choose $g'(m)=g(m)+(1/2)[g(m-1)+g(m+1)]$; and according to (9c), I,Q-separately SVA would do the same. So we see that in all cases, for Nyquist-sampled imagery in one dimension, CDA employing uniform and Hanning weightings is identical to I,Q-separately SVA.

ACKNOWLEDGMENTS

We are grateful to Wright Laboratory for the DCS image, and to J. C. Dwyer for helpful discussions in formulating the I,Q jointly SVA approach. K. Mangis provided the program used to generate the image example.

REFERENCES

[1] Ausherman, D. A., Kozma, A., Walker, J. L., Jones, H. M., and Poggio, E. C. (1984)
Developments in radar imaging
IEEE Transactions on Aerospace and Electronic Systems, **AES-20**, 4 (1984), 363–400.

[2] Harris, F. J. (1978)
On the use of windows for harmonic analysis with the discrete Fourier transform.
Proceedings of the IEEE, **66**, 1 (Jan. 1978).

[3] Hecht, E., and Zajac, A. (1975)
Optics.
Reading, MA: Addison-Wesley, 1975.

[4] Walker, J. L. (1980)
Range-Doppler imaging of rotating objects.
IEEE Transactions on Aerospace and Electronic Systems, **AES-16**, 1 (Jan. 1980), 23–52.

[5] Crowe, D. G., Shamir, J., and Ryan, T. W. (1993)
Sidelobe reduction in optical signal processing.
Applied Optics, **32**, 2 (Jan. 10, 1993), 179–183.

[6] Stankwitz, H. C., Dallaire, R. J., and Fienup, J. R. (1994)
Spatially variant apodization for sidelobe control in SAR imagery.
1994 IEEE National Radar Conference.

[7] Dallaire, R. J., and Stankwitz, H. C. (1994)
Spatially variant apodization.
U.S. Patent No. 5,349,359, Sept. 20, 1994.

Herbert C. Stankwitz was born in Mt. Pleasant, MI, on Aug. 25, 1954. He received the B.S.E. degree in electrical engineering from the University of Michigan, Ann Arbor, in 1976, and the M.S.E. degree in control systems engineering from UCLA in 1980 under sponsorship of the Hughes Aircraft Co. fellowship program.

He worked at Hughes Aircraft Co., Missile Systems Group, from 1977 to 1985 on guidance and control of radar-guided, air-to-air missiles. Since that time, he has been employed by the Environmental Research Institute of Michigan, working on advanced SAR system design and image processing techniques. Mr. Stankwitz has one patent.

Rodney J. Dallaire was born in Detroit, MI on Oct. 4, 1946. He received a B.S. in electrical engineering in 1970 and an M.S. in computer information, and control engineering in 1973, both from the University of Michigan, Ann Arbor.

He is with the Environmental Research Institute of Michigan where he has spent the last 20 years specializing in SAR systems engineering. He has managed and conducted research in the areas of SAR systems analysis, simulation, digital image processing, pattern recognition, and image exploitation. He is currently a senior staffer in the Advanced Systems Program. Prior to the Environmental Research Institute of Michigan, he worked as an engineer for the Bendix Aerospace Corporation.

Mr. Dallaire has two patents.

James R. Fienup (M'85—SM'91) received B.A. degrees in physics and mathematics (magna cum laude) from Holy Cross College, Worcester, MA in 1970, and the M.S. and Ph.D. degrees in applied physics from Stanford University, Stanford, CA, in 1972 and 1975, respectively. He was a National Science Foundation Graduate Fellow from 1970 to 1972.

He is currently the Senior Scientist in the Optical & IR Science Laboratory of the Environmental Research Institute of Michigan (ERIM), which he joined in 1975. His research activities include phase retrieval and image reconstruction, optical and digital image processing for synthetic aperture radar, and holographic optical elements.

He is a fellow of the Optical Society of America and of the International Society for Optical Engineering (SPIE). He is the recipient of the SPIE 1979 Rudolph Kingslake Medal and Prize, the International Commission for Optics 1983 International Prize in Optics, and the Best Paper Award for 1990 by the IRIS Specialty Group on Active Imaging. He has served as associate editor of *Optics Letters*, three times as a feature editor of the *Journal of the Optical Society of America A*, and on NASA's Hubble Space Telescope Image Processing Working Group. His publications include over 90 papers and he has three patents.